IEEE Access
Multidisciplinary | Rapid Review | Open Access Journal

Received November 14, 2019, accepted November 22, 2019, date of publication November 26, 2019,
date of current version December 12, 2019.

Digital Object Identifier 10.1109/ACCESS.2019.2955957

A Convolutional Neural Network Using Surface Data to Predict Subsurface Temperatures in the Pacific Ocean

MINGXU HAN[1], YUAN FENG[1], XUELI ZHAO[1], CHUNJIAN SUN[2], FENG HONG[1], (Member, IEEE), AND CHAO LIU[1]

[1]College of Information Science and Engineering, Ocean University of China, Qingdao 266100, China
[2]National Marine Data Information Center, Tianjin 300000, China

Corresponding author: Yuan Feng (fengyuan@ouc.edu.cn)

This work was supported in part by the National Research and Development Program of China under Grant 2016YFC1401900, in part by the Open Foundation of Qingdao National Laboratory for Marine Science and Technology under Grant QNLM20160RP0405, and in part by the National Natural Science Foundation of China under Grant 61902367 and Grant 41976185.

ABSTRACT This paper proposes a convolutional neural network (CNN) method to estimate subsurface temperature (ST) in the Pacific Ocean from a suite of satellite remote sensing measurements. These include sea surface temperature(SST), sea surface height (SSH), and sea surface salinity (SSS). We propose using the multisource sea surface parameters to establish a monthly CNN model to reconstruct the ocean subsurface temperature (ST) and use Argo data for accurate validation. The results show that the CNN can accurately estimate the ST of the Pacific Ocean by using the model. We trained the model for 12 months. The most prominent months are January, April, July, and October with average mean square error (MSE) values of 0.2659, 0.3129, 0.5318, and 0.5160, and the average coefficients of determination (R^2) were 0.968, 0.971, 0.949, and 0.967, respectively. This study improves the accuracy of ST estimation and the good results based on reanalysis indicate that the model is promising to be applied to satellite observations.

INDEX TERMS Convolutional neural network, ocean data, satellite measurements, subsurface temperature.

I. INTRODUCTION

The roles of oceans as huge reservoirs of heat and water are important in the global climate system [1]. The accurate detection and description of the subsurface thermal structure of the global ocean is an important aspect of ocean dynamics. Subsurface data are critical for understanding the mechanisms and processes in the ocean as a whole, as well as for the entire Earth climate system [2]. According to research evidence, the thermocline in the equatorial Pacific will remain abnormally deep for a long time [3]. This not only causes the warming of the eastern equatorial Pacific to be greater than that outside of the equatorial region but also causes the sea surface temperature gradient to weaken, which is one of the main mechanisms that leads to the frequent occurrence of extreme El Niño events [4]. The Intergovernmental Panel on Climate Change (IPCC) reported that the global average SST will increase by about approximately 0.20°C per decade [5]. Therefore, the determination of SST and ST is one of the most important issues in climate science for studying El Niño events and how they respond to greenhouse warming [6].

Satellite remote sensing technologies have collected multiple sea surface observations at various spatiotemporal scales, but these technologies are confined to ocean surface layers. Because significant dynamic processes and features are located at much greater depths below the surface, and existing data cannot describe the internal structure of the ocean completely and accurately, it is very necessary to construct a complete three-dimensional thermohaline structure [7]. With the continuous development of satellite remote sensing technology, especially SST and SSS data from satellite remote sensing, a large amount of real time information of the sea surface is produced with wide coverage, high precision and spatial resolution, and strong time continuity. Determining how to use the data obtained by satellite remote sensing to predict the surface information of the ocean, and establish a complete set of three-dimensional analysis and prediction systems for the surface is an urgent problem to be solved in the field of international marine research.

The associate editor coordinating the review of this manuscript and approving it for publication was Aysegul Ucar.

Ali used an artificial neural network (ANN) approach to estimate temperature structures from SST, SSH, wind stress, net radiation, and net heat flux, all available from an Arabian Sea mooring. On average, 50% of the estimations were within ±0.50°C error and 90% were within ±1.00°C error [8]. For a temperature field at a depth of 200 m in the North Atlantic, S.Guinehut estimated oceanic three-dimensional temperature fields using multiple linear regression combined with Argo and remote sensing data, and used objective analysis methods. The root mean square error (RMSE) of the mapping error of large-scale and low-frequency temperature fields at 200 m depth was largely reduced by combining both data sets compared to the results obtained using only in situ profiles [9].

Takano proposed a new empirical method to estimate mesoscale three-dimensional oceanic thermal structures from near-real-time satellite altimetry data. The method uses a two-layer model with a novel set of empirical parameters for stratification [10]. Wu used a self organizing map (SOM) neural network to estimate subsurface temperature anomalies in the North Atlantic using SST, SSH, and SSS data from the Argo monthly anomaly grid dataset. This method shows good performance at depths of 30 to 700 m with a correlation coefficient greater than 0.80 [2].

Patil predicted ocean temperature using a combination of numerical and artificial network techniques. The error statistics for daily forecasts are r (coefficient of correlation) = 0.37, RMSE = 0.47°C and MAE (mean absolute error) = 0.38°C. The weekly forecasted error statistics are r = 0.27, RMSE = 0.78°C and MAE = 0.64°C, and the monthly forecast error statistics are r = 0.11, RMSE = 0.58°C and MAE = 0.46°C [11].

Su proposed a support vector machine method that can accurately estimate the subsurface temperature anomaly (STA) in the upper 1000 m of the Indian Ocean from satellite measurements of sea surface parameters. The results were reliable with reasonable accuracy as validated using Argo STA data. The estimation accuracy gradually decreased as depth increased to deeper than 500 m [12]. Su proposed a new approach based on random forest (RF) machine learning to retrieve the STA in the global ocean from multisource satellite observations including SSH, SST, SSS, and SSW via in situ Argo data for RF training and testing. The RF optimized R^2 was 0.630 at 125 m. The RF R^2 was 0.045 greater than that of the SVR model [7]. Su et al. (2018) developed a new satellite-based geographically weighted regression (GWR) model for inversion of the Indian Ocean subsurface temperature structure. The final experimental result was that the RMSE range was approximately 0.10 to 0.18, and the R^2 range was approximately 0.50 to 0.80 [13].

Lu et al proposed a new method that combines a pre-clustering process and a neural network (NN) approached to determine the STA using ocean surface temperature, surface height, and surface wind observation data at the global scale. Results show that the best estimation resulted in an overall root-mean-squared error of 0.41 °C and a determination coefficient (R^2) of 0.91 at the 50 m level for all months. The R^2 decreased to 0.51 at 300 m but was still better than the calculation without pre-clustering [14].

Su et al proposed a new ensemble learning algorithm, extreme gradient boosting (XGBoost), for retrieving subsurface thermohaline anomalies, including the subsurface temperature anomaly (STA) and the subsurface salinity anomaly (SSA), in the upper 2000 m of the global ocean. The XGBoost model had good performance with average R^2 value of 0.69, and average normalized root-mean-square error (NRMSE) value of 0.035, for STA estimations, respectively [15].

The large SST annual cycle in the eastern equatorial Pacific is, to a large extent, controlled by the annually varying mixed layer depth which, in turn, is mainly determined by the competing effects of solar radiation [16] and wind forcing [17]. There is spring instability of SST anomalies both in the tropical and extratropical Pacific. This instability is crucial for the existence of a predictability barrier for an El Niño event [18].

Under the influence of global warming, the mean climate of the Pacific region will probably undergo significant changes. In the past, researchers built data prediction models in annual units, which were affected by climate and seasonal variations. These data prediction models usually needed to subtract the climatic average to eliminate the impact on the training model, but the results showed that the ST predictive ability was insufficient. This study proposes to establish a monthly data model to eliminate the impact of climate on model training. The results show that the accuracy of STA prediction is significantly improved. Researchers have used single-point features to establish STA prediction models, which did not consider the influence of seawater flow or ocean currents on seawater heat transfer. In this research, the characteristics of 624 data points closest to the predicted point are selected to train the model, which makes full use of the multi-source parameter data of the ocean surface.

In summary, ocean surface remote sensing observation data are being used to estimate dynamic environmental information about the ocean more frequently. Existing approaches for retrieving subsurface thermal structures from sea surface parameters are generally based on either dynamic models or statistical models. Existent dynamic approaches rarely focus on global-scale application and advanced machine learning models and employ only a few surface parameters to derive subsurface dynamic fields. Thus, the estimation methods themselves and their global-scale accuracy still show much room for improvement. The shortcomings of current statistical methods are the inadequate use of ocean surface data features, single features, large annual models affected by climate, and no deep learning models. These factors all lead to poor predictions by this method.

A basic method for estimating the thermal structure information of the ocean subsurface is usually combined with a dynamic model that uses in-situ observations or a statistical relationship model that is based solely on sea surface and subsurface parameters. However, past statistical methods have relied more on regression analysis for spatial modeling

and on the application of simple traditional machine learning algorithms. This is not sufficient for the application of ocean surface data parameters and lacks the application of deep learning models. In addition, the input characteristics of the models are relatively few in number, the feature quantity is insufficient, and the learning ability is poor. The models based on annual data are greatly affected by the climate, and the monthly positive and negative temperature difference is large. Researchers must subtract the climatic average of their respective characteristics to eliminate the impact of climate variability on model training, but this still cannot eliminate the impact of error, making the previous estimation models lacking and warranting a need for improved accuracy.

This study is based on the Pacific Ocean and uses a CNN method. Based on multisource satellite observation data, this method uses the surrounding, most correlated data points to predict the center point ST. An experiment was constructed for 12 different months using the CNN model to estimate the ST in the Pacific. This model improves the prediction accuracy of ST and provides data support for the construction of deeper ocean data sets in the Pacific Ocean and Pacific warming analysis.

II. STUDY AREA AND DATA

A. RESEARCH AREA OVERVIEW

The Pacific Ocean is the largest of the four oceans on the planet. It extends from the Arctic Ocean to the Southern Ocean. It faces Asia and Oceania to the west and the Americas to the east. The heat and dynamics of the ocean and atmosphere are complex and variable. This ocean is the engine and regulator of the global climate system. Frequent occurrences of the El Niño and La Niña events in the eastern and eastern equatorial Pacific have caused extreme weather events around the world, which have a tremendous impact on ecosystems and agriculture [19].

Reconstructing the ocean subsurface temperature profile from the Pacific sea surface information obtained by satellite remote sensing is of great significance to the study of global warming, El Niño and La Niña events. The area of the Pacific Ocean studied in this paper is located between 60.50° S and 50.50° N, 64.50 ° W and 100.50° E.

B. DATA (1) GLORYS2V4 REANALYSIS (2) BOA-Argo

The GLORYS2V4 REANALYSIS data and Argo measured data used in this study are as follows:

(1) The satellite sea surface temperature (SST) is from Advance Very High Resolution Radiometer (AVHRR) dataset with spatial resolution of 0.25° × 0.25° and monthly temporal resolution (https://www.ncdc.noaa.gov/oisst/data-access) [20].

The multi-satellites merged Sea Surface Height (SSH) data is obtained from Archiving, Validation and Interpretation of Satellite Oceanographic data (AVISO), which has spatial resolution of 0.25° × 0.25° and monthly temporal resolution (https://www.aviso.altimetry.fr/en/data/products/sea-surface-height-products.html) [21].

The above data is used by COPERNICUS MARINE ENVIRONMENT MONITORING SERVICE (CMEMS) for quality control reanalysis using The Mercator Ocean (Toulouse, FR) GLORYS2V4 reanalysis (http://marine.copernicus.eu/services-portfolio/access-to-products/?option=com_csw&view=details&product_id=GLOBAL_REANALYSIS_PHY_001_025).

(2) Field observations of Argo data for labels in model training and validation. The Argo hierarchical observation dataset product is used in this study. There are 57 standard layers from 5 m to 1975 m depth. Each layer includes observations such as temperature, and salinity. The time span is from 2004 to 2015 [22].

We reanalyzed the observations that absorbed these satellites. Good results based on reanalysis indicate that the model is expected to be used for satellite observations. we try to make use of the characteristics of remote sensing data sets, such as easy access, large amount of data and high accuracy, and combined the data with Argo measured dataset to establish a large-scale ocean subsurface temperature prediction model.

C. DATA PREPROCESSING

This study used data sets from 2004 to 2015 for model training and evaluation, where the 2005 to 2014 data sets were used for model building and the 2004 and 2015 data sets were used for model evaluation. From 2005 to 2014, the data set was divided into 12 different data sets by month, and 12 sets of monthly CNN models were established. Each group of model data has 140,000 samples, of which 78,400 (56%) were used to train the data model, 19,600 (14%) were used to validate the model, and 42,000 (30%) were used to test the model.

This study standardizes the ocean surface features, which ensures that the dimensions and magnitudes of different features have the same range of values. The features of a single sample are subtracted from the average of all training samples (same features) and then divided by the variance of all training samples. Thus, for each feature, all data are clustered around 0 with a variance of 1. The specific calculations are as follows:

$$\mathrm{X\ (normalization)} = \frac{x - \mu}{\sigma} \tag{1}$$

where x is the training sample and the test set single sample feature value, μ is the average of the training sample data, σ is the standard deviation of the training sample data, and X is the normalized feature value.

This study relates the temperature data of the center point of Argo to the corresponding position of the GLORYS2V4 REANALYSIS data according to the coordinates of longitude and latitude, which eliminates the influence of GLORYS2V4 REANALYSIS data and Argo resolution mismatch (GLORYS2V4 REANALYSIS data resolution is

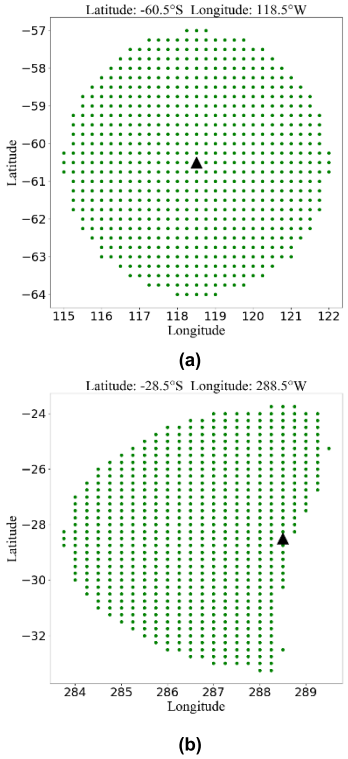

FIGURE 1. The selected data characteristics of multisource sea surface parameters obtained by satellite remote sensing observations. Point a is at −60.50° S, 118.50° E; point b is at −28.50° S, 288.50° W; and the spatial resolution is 0.25° × 0.25°.

0.25° × 0.25°, and Argo resolution is 1° × 1°, unified to 0.25° × 0.25°).

Figure 1 shows the range of data feature selections for central point a (−60.50° S, 118.50° E) and coastal data point b (−28.50° S, 288.50° W). In this research, the selected training feature was the center point and the 624 data points closest to the center point. (625 data points, 1875 features). The selected features that are far from the coastline can better form a circular region, but near the coast, because of the existence of land areas, a circular region cannot be formed. Therefore, we used the distance formula (2) between two points to calculate the 624 data points closest to the center point as data features.

$$|d_i| = \sqrt{(x_0 - x_i)^2 - (y_0 - y_i)^2} \quad (1 < i \leq 625) \qquad (2)$$

where i is the current data point (1 < i <= 625). x_0 represents the longitude of the center point, and y_0 represents the dimension. d_i is the distance of the current i point from the center point (x_0, y_0). Finally, we calculated and filtered out the 624 data points closest to the center point (x_0, y_0).

III. METHODOLOGY

A. CONVOLUTIONAL NEURAL NETWORK

Convolutional neural network (CNN) have more complex network structures and more powerful feature learning and feature representation capabilities than traditional machine learning methods [25]. Each neuron is treated as a filter, its receptive field is slid, and a filter is used to calculate local data. A rectified linear unit (RELU) excitation layer performs a nonlinear mapping operation on the result of the convolutional layer output. The pooled layer is sandwiched between successive convolutional layers and is used to compress the amounts of data and parameters, reducing overfitting. Usually the fully connected layer is at the end of the convolutional neural network, which is the same as the connection for traditional neural network neurons [23].

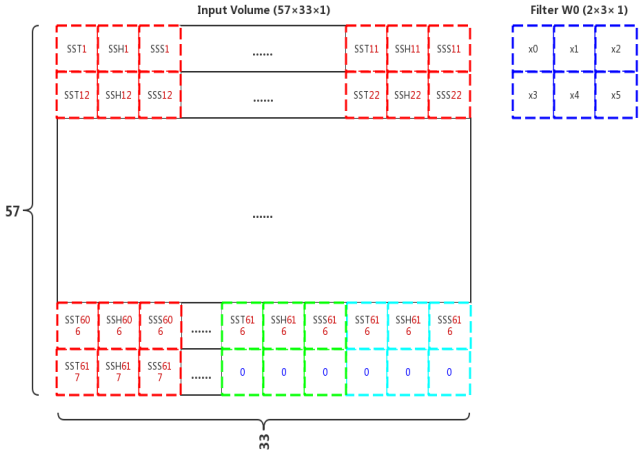

FIGURE 2. A single training sample (57 × 33) performs a 2 × 3 partial convolution operation. (SST_1, SSH_1, SSS_1) – (SST_{625}, SSH_{625}, SSS_{625}) represent the characteristics of 1-625 grid points. 0 represents the value 0. x_0-x_5 represents the random number of the 2 × 3 convolution kernel.

A disadvantage of CNN lies in the parameter update being slow, which requires a great deal of time to adjust the parameters and network layer according to the experimental observations. To reduce the data dimension, the pooling layer is often added, which leads to the loss of much very valuable information. A CNN always activates a small range of data for calculation, which ignores the relationship between the whole and the part. The applicability of CNN lies in the ability to share weights, so the network depth of a CNN is not limited by the expansion of parameters.

An advantage of CNN lies in the shared convolution kernel, which is efficient for processing high-dimensional data, and can automatically extract some advanced features, reducing the time of feature engineering [24], which can improve the accuracy of predicting subsurface temperature. Therefore, we propose to use a CNN to construct the model by using the characteristics of 624 data points closest to the predicted point, which significantly related to practical feasibility.

B. EXPERIMENTAL SETUP

The data point with the center point and the 624 data points closest to the center point are treated as a two-dimensional image, that performs a convolution operation for the local field of view, and the three features (SST, SSH, and SSS) of each data point are operated in one convolution unit. The RELU activation and Adam optimization functions are used.

Figure 2 shows the set CNN network structure, which consists of a 5 layer convolution operation, followed by a

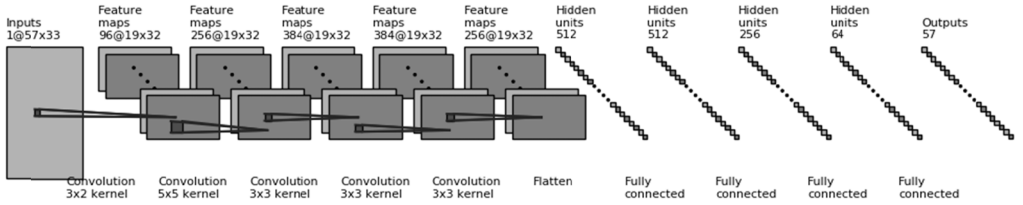

FIGURE 3. CNN structure, including 5 convolution operation layers and 4 fully connected layers.

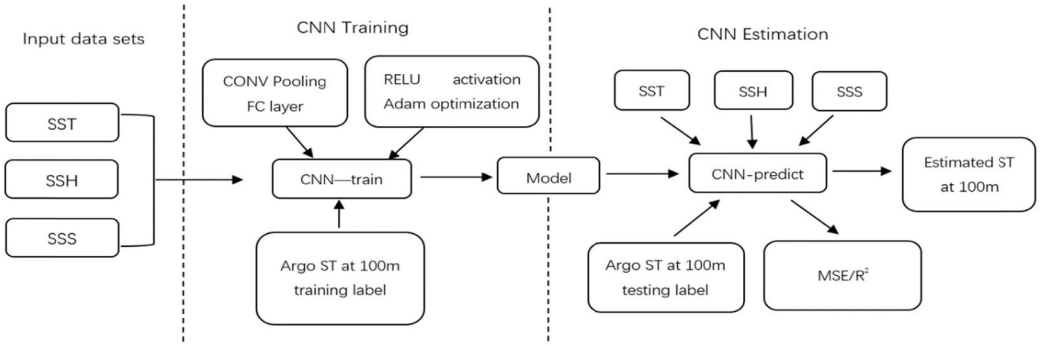

FIGURE 4. Flow chart for determining the ST in the Pacific Ocean by the CNN model using the sea surface multisource remote sensing observation data (100 m).

4 layer fully connected layer. The stride of the first layer of the convolution layer is (3,1); that is, Figure 3 the horizontal direction moves by 3 steps, the vertical direction moves by 1 step, and the size of the filter is 3 × 2. In other words, the features (SST, SSH, and SSS) of the two data points are multiplied by the corresponding elements of the filter, and then a sum is obtained. After calculating one block area, the specified stride (3, 1) is moved to other areas until a two-dimensional matrix (57 × 33) is completely covered. After the 5 layer convolution operation, the data dimension is tiled into one-dimensional data, input to the fully connected layer and then subjected to a 4 layer neural network operation. Finally, 57 layers of predicted values are output.

Figure 4 shows the process of estimating the Pacific ST by establishing a monthly CNN model from sea surface multi-source remote sensing observation data (SST, SSH, and SSS) (100 m).

First, a training dataset is built. The selected training feature was the surrounding data points with the center point and the 624 data points closest to the center point (625 data points, 1875 features). Argo-measured ST are used as training markers and test markers, and all datasets are standardized.

Second, the CNN model is trained, and an optimal CNN model is built. The model uses RELU as the activation function and Adam as the optimization function. We determined the optimal combination of the convolutional layer, pooled layer, and fully connected layer by analyzing each MSE, R^2, and convergence speed. We used the training data sets (SST, SSH, and SSS) as input data for CNN training, and the Argo ST was used as the training marker.

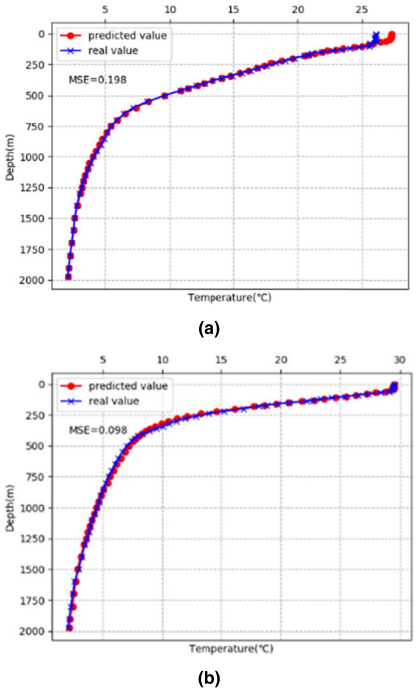

FIGURE 5. Comparison of temperatures at different depths (5 m-1975 m) by the CNN single-point prediction and Argo measured at near-coast point a (21.50° N, 122.50° E) and far-coast point b (14.50° N, 160.50° E). CNN predicted value Argo measured value in October 2015.

Finally, we used the data sets (SST, SSH, SSS) as the input parameters of the CNN model to predict the ST. We used the ST measured by Argo to evaluate the prediction accuracy of the CNN model at each level of the subsurface (57 layers).

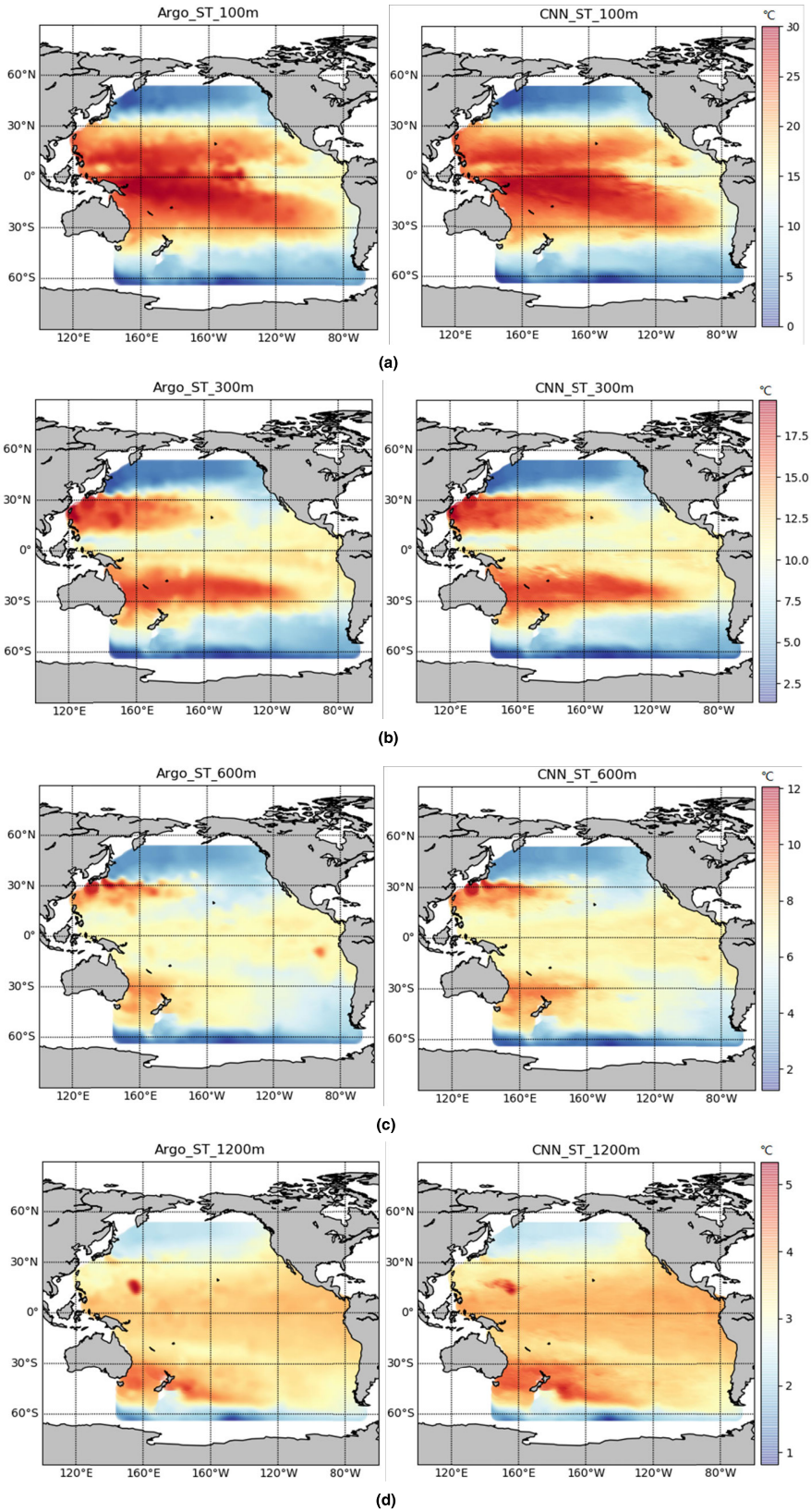

(I) The Pacific ST regional distributions predicted by the CNN and measured by Argo at 100 m(a), 300 m(b), 600 m(c), and 1200 m(d) depth in April 2015.

FIGURE 6. ST estimated by the CNN and the corresponding measured Argo ST in different depth horizons (100 m, 300 m, 600 m, and 1200 m) in different months (4(I)/10(II)) in 2015.

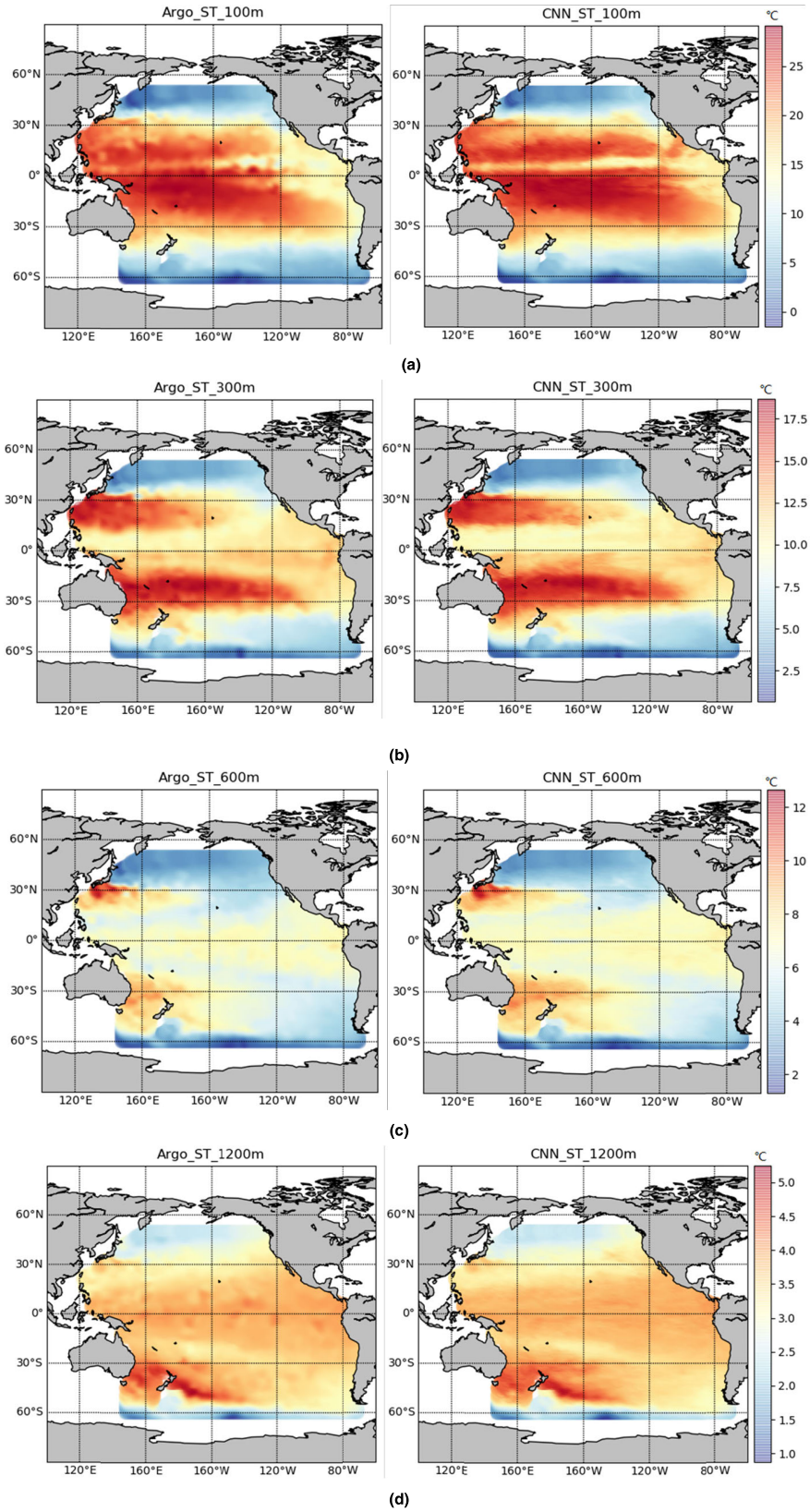

(II) The Pacific ST regional distributions predicted by the CNN and measured by Argo at 100 m(a), 300 m(b), 600 m(c) and 1200 m(d) depth in October 2015.

FIGURE 6. *(Continued.)* **ST estimated by the CNN and the corresponding measured Argo ST in different depth horizons (100 m, 300 m, 600 m, and 1200 m) in different months (4(I)/10(II)) in 2015.**

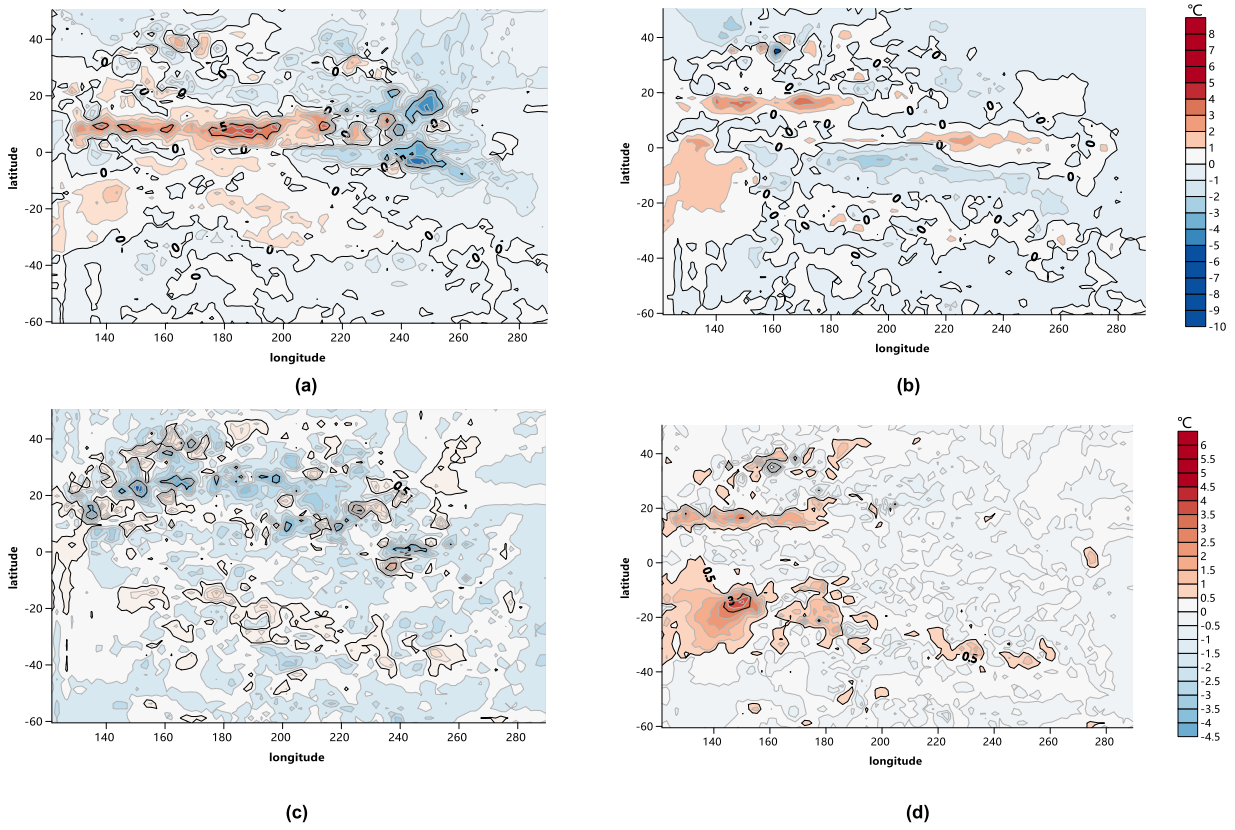

FIGURE 7. Isotherm plots of the error values of the Argo measured values and the CNN predicted values in the Pacific region at different depths(100 m(a, c),300 m(b, d)) in October 2015(a, b) and 2004(c, d).

IV. RESULTS AND DISCUSSION

A. OVERALL SPATIAL RESULT

Figure 5 shows a comparison of the true and predicted values of the two different depth horizons of the near-coastal point a (21.50° N, 122.50° E) and the far-shore point b (14.50° N, 160.50° E) in October 2015. The results show that the model trained by the method of predicting the center point and the 624 data points closest to the center point not only has a good prediction effect on the rule-associated data points at the far coast but also has a good prediction effect for the data points with irregular associations near the coast. The prediction effect indicates that the model also has generalization ability for irregular data points on the coast.

Figure 6 shows that the ST of the measured values from Argo at different depths (100 m, 300 m, 600 m, and 1200 m) in different months (4/10) show good agreement with the ST estimated using the CNN, and the predicted anomalous regions and the distribution patterns are more consistent.

Figure 7 shows that the measured values from Argo in the El Niño area (5° S–5° N, 160° E-90° W) at 100 m and 300 m in October 2015 are much higher than the CNN predictions. The contour plot error was higher than the values at 100 m and 300 m in October 2004. This was due to the extremely intense El Niño phenomenon in 2015, which caused the sea temperature in the equatorial central and eastern Pacific Ocean to rise substantially. This proves that the CNN model has a reduced ability to predict abnormal years. Abnormal information cannot be perceived due to the insufficient amount of data in an abnormal year. We hope to further study abnormal year information by collecting more data sets of abnormal years.

Low-temperature seawater in the tropical Pacific Ocean is obviously at different depths, especially at depths of 100 m to 300 m, which is related to La Niña events in the upper layer of the tropical Pacific that occur in March and April. The ST at different depths in the tropical Pacific Ocean are significantly lower than in other oceans. As the depth increases, the seawater temperature tends to be stable overall, the magnitude of ST change decreases, and the spatial heterogeneity gradually declines, which is related to the difference between the ocean interior and the surface dynamics.

B. OVERALL ERROR RESULT

Figure 8 shows at R^2 and normalized root mean squared error (NRMSE) comparison of the 12 different month models from training at different depths in 2004. The NRMSE evaluation indicator reflects that our predictions have less residual variation. We select the months (1,4,7,10) with significant changes in ocean climate as the analytical data. These are shown in Table 1 and 2 and Figure 9. In January, April, July and October of 2004 and 2015,

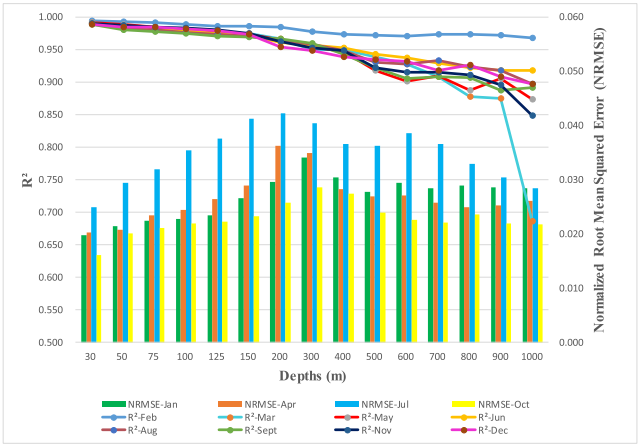

FIGURE 8. An R^2 and NRMSE comparison of the 12 different month models from training at different depths in 2004.

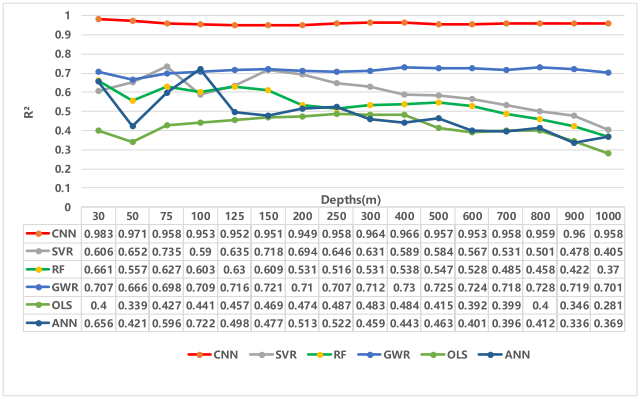

Depths(m)	30	50	75	100	125	150	200	250	300	400	500	600	700	800	900	1000
CNN	0.983	0.971	0.958	0.953	0.952	0.951	0.949	0.958	0.964	0.966	0.957	0.953	0.958	0.959	0.96	0.958
SVR	0.606	0.652	0.735	0.59	0.635	0.718	0.694	0.646	0.631	0.589	0.584	0.567	0.531	0.501	0.478	0.405
RF	0.661	0.557	0.627	0.603	0.63	0.609	0.531	0.516	0.531	0.538	0.547	0.528	0.485	0.458	0.422	0.37
GWR	0.707	0.666	0.698	0.709	0.716	0.721	0.71	0.707	0.712	0.73	0.725	0.724	0.718	0.728	0.719	0.701
OLS	0.4	0.339	0.427	0.441	0.457	0.469	0.474	0.487	0.483	0.484	0.415	0.392	0.399	0.4	0.346	0.281
ANN	0.656	0.421	0.596	0.722	0.498	0.477	0.513	0.522	0.459	0.443	0.463	0.401	0.396	0.412	0.336	0.369

FIGURE 9. Comparison of R^2 values for different algorithm models.

the MSE is the highest when the depth horizon is 30 m to 200 m (the highest MSE value is 0.8408/1.1034/1.8640/2.8231/0.5961/0.6750/1.1856/0.4788), which may be related to the complex dynamic process of the upper Pacific Ocean and the disturbance of the mixed layer and thermocline [26].

Figure 9 shows a comparison of the R^2 value of the CNN method used in this experiment with that of other traditional machine learning algorithms.

The proposed CNN method has higher prediction accuracy than other machine learning algorithms, such as support vector regression (SVR), random forest (RF), geographically weighted regression (GWR), ordinary least squares (OLS).

Figure 10 shows that the MSE slightly decreases below a depth of 300 m, and the R^2 values decreases steadily, which reflects the model predictive power decline. This may be because the stratification of the middle and deep seawater is relatively stable, and a physical phenomenon inside the ocean is harder to predict with surface features. From Table 1 and 2, it can be concluded that the prediction accuracy of the model is not similar in different years and months.

(1) In the same year, using the 100 m depth from 2015 as an example, the average MSE in January is 0.2821

TABLE 1. Comparison of MSE and R2 values corresponding to CNN models at different depths (18 levels) in 2015.

Depths/m 18 levels	201501		201504		201507		201510	
	MSE	R^2	MSE	R^2	MSE	R^2	MSE	R^2
30	0.4069	0.993	0.6562	0.990	0.5279	0.993	1.1458	0.983
70	0.7532	0.987	1.1034	0.982	1.5804	0.975	2.8232	0.958
100	0.8408	0.985	1.0011	0.982	1.8640	0.966	2.7928	0.953
130	0.7907	0.984	0.8335	0.983	1.6129	0.964	2.3136	0.953
160	0.7078	0.982	0.7220	0.982	1.7304	0.952	1.9425	0.950
200	0.4524	0.984	0.5637	0.980	1.3466	0.949	1.4407	0.949
260	0.3128	0.983	0.3737	0.979	0.8257	0.954	0.7725	0.958
300	0.2482	0.982	0.2717	0.981	0.6367	0.955	0.5162	0.964
400	0.1575	0.978	0.1832	0.976	0.3943	0.946	0.2513	0.966
500	0.1310	0.965	0.1546	0.962	0.2539	0.934	0.1670	0.957
600	0.0887	0.958	0.1091	0.953	0.1472	0.933	0.1030	0.953
700	0.0591	0.958	0.0593	0.958	0.0767	0.946	0.0599	0.958
800	0.0432	0.958	0.0378	0.963	0.0521	0.950	0.0416	0.959
900	0.0308	0.959	0.0295	0.961	0.0412	0.948	0.0299	0.960
1000	0.0252	0.954	0.0225	0.959	0.0325	0.944	0.0231	0.958
1200	0.0157	0.944	0.0123	0.958	0.0225	0.923	0.0138	0.950
1400	0.0081	0.944	0.0064	0.957	0.0172	0.888	0.0087	0.940
1800	0.0062	0.891	0.0041	0.926	0.0095	0.842	0.0034	0.939
Average	0.2821	0.966	0.3413	0.968	0.6207	0.942	0.8027	0.956

TABLE 2. Comparison of MSE and R^2 values corresponding to CNN models at different depths (18 levels) in 2004.

Depths/m 18 levels	200401		200404		200407		200410	
	MSE	R^2	MSE	R^2	MSE	R^2	MSE	R^2
30	0.3406	0.994	0.3663	0.995	0.6205	0.991	0.2744	0.996
70	0.4948	0.992	0.4930	0.992	0.9992	0.985	0.4614	0.993
100	0.5158	0.991	0.5427	0.990	1.1726	0.980	0.4788	0.992
130	0.5502	0.989	0.6265	0.987	1.1855	0.976	0.4679	0.990
160	0.5935	0.985	0.6750	0.983	1.1662	0.970	0.4368	0.989
200	0.4945	0.982	0.6626	0.977	0.8548	0.970	0.3809	0.987
260	0.4069	0.977	0.5669	0.969	0.5781	0.968	0.3160	0.983
300	0.3230	0.977	0.4145	0.971	0.4748	0.966	0.2703	0.981
400	0.1774	0.975	0.1925	0.975	0.3111	0.957	0.1714	0.977
500	0.1030	0.972	0.1277	0.969	0.1999	0.947	0.1121	0.971
600	0.0686	0.968	0.0870	0.963	0.1250	0.942	0.0701	0.968
700	0.0477	0.966	0.0480	0.967	0.0774	0.945	0.0390	0.972
800	0.0364	0.964	0.0305	0.970	0.0476	0.953	0.0252	0.975
900	0.0272	0.964	0.0249	0.967	0.0346	0.955	0.0174	0.977
1000	0.0234	0.957	0.0196	0.965	0.0261	0.953	0.0133	0.976
1200	0.0134	0.952	0.0112	0.961	0.0149	0.948	0.0078	0.972
1400	0.0064	0.956	0.0058	0.961	0.0125	0.916	0.0049	0.966
1800	0.0055	0.903	0.0034	0.940	0.0085	0.853	0.0026	0.954
Average	0.2349	0.970	0.2721	0.972	0.4394	0.954	0.1972	0.979

TABLE 3. Comparison of RMSE values corresponding to CNN models at different depths (18 levels) in 2004 and 2015.

Depths/m 18 levels	1		4		7		10	
	2015	2004	2015	2004	2015	2004	2015	2004
30	0.6379	0.5836	0.8101	0.6052	0.7266	0.7877	1.0704	0.5239
70	0.8679	0.7034	1.0504	0.7021	1.2571	0.9996	1.6802	0.6792
100	0.9170	0.7182	1.0005	0.7367	1.3653	1.0829	1.6712	0.6919
130	0.8892	0.7418	0.9129	0.7915	1.2700	1.0888	1.5211	0.6840
160	0.8413	0.7704	0.8497	0.8216	1.3155	1.0799	1.3937	0.6609
200	0.6726	0.7032	0.7508	0.8140	1.1604	0.9246	1.2003	0.6172
260	0.5593	0.6379	0.6113	0.7530	0.9087	0.7603	0.8789	0.5622
300	0.4982	0.5683	0.5213	0.6438	0.7980	0.6890	0.7185	0.5199
400	0.3968	0.4212	0.4280	0.4387	0.6279	0.5578	0.5013	0.4141
500	0.3619	0.3210	0.3932	0.3574	0.5039	0.4471	0.4086	0.3348
600	0.2978	0.2620	0.3303	0.2949	0.3837	0.3536	0.3209	0.2648
700	0.2431	0.2183	0.2436	0.2191	0.2770	0.2781	0.2447	0.1974
800	0.2079	0.1907	0.1945	0.1746	0.2283	0.2181	0.2040	0.1587
900	0.1755	0.1650	0.1716	0.1579	0.2030	0.1861	0.1730	0.1319
1000	0.1587	0.1531	0.1501	0.1402	0.1804	0.1616	0.1521	0.1153
1200	0.1253	0.1157	0.1109	0.1060	0.1501	0.1220	0.1176	0.0885
1400	0.0902	0.0800	0.0800	0.0760	0.1312	0.1120	0.0934	0.0700
1800	0.0788	0.0742	0.0641	0.0580	0.0974	0.0921	0.0586	0.0510
Average	0.4455	0.4127	0.4819	0.4384	0.6436	0.5523	0.6894	0.3759

(maximum/minimum is 0.8408/0.0062) and the average R^2 value is 0.966 (maximum/minimum is 0.993/0.891). The MSE (R^2) in January is less (greater) than that in April, July and October, indicating that the estimation accuracy improved, which is related to seasonal influence. The temperature of the seawater in the winter tends to be stable, and the magnitude of ST changes is small. In July and October, due to the obvious change in seawater temperature in summer and autumn, the Pacific Ocean is heavily affected

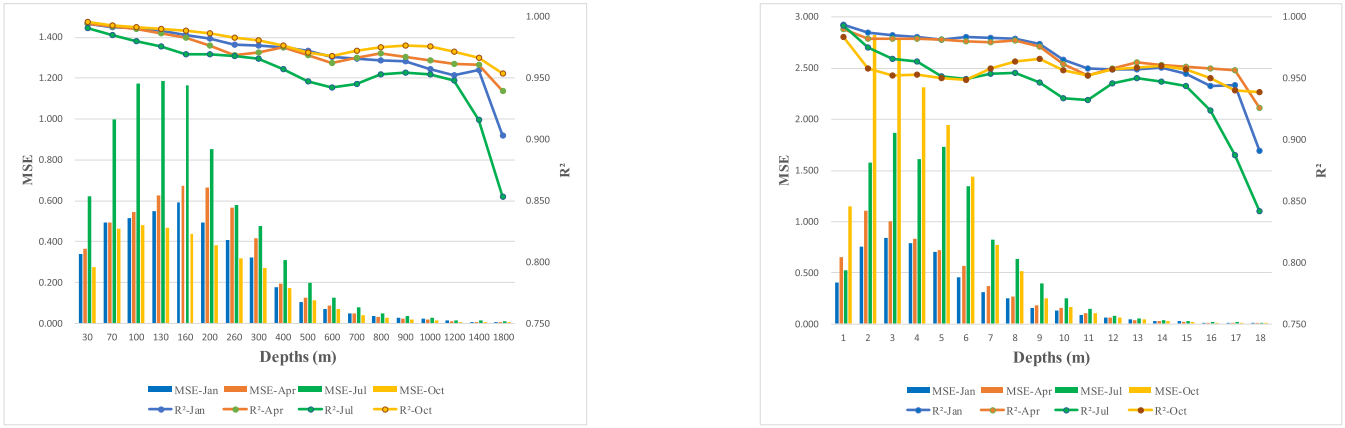

FIGURE 10. Accuracy evaluation of 18 different depth horizon ST estimates in the Pacific Ocean in January, April, July and October of 2004 (a) and 2015 (b) based on the CNN model in 2004 and 2015 (evaluation indexes using MSE and R^2).

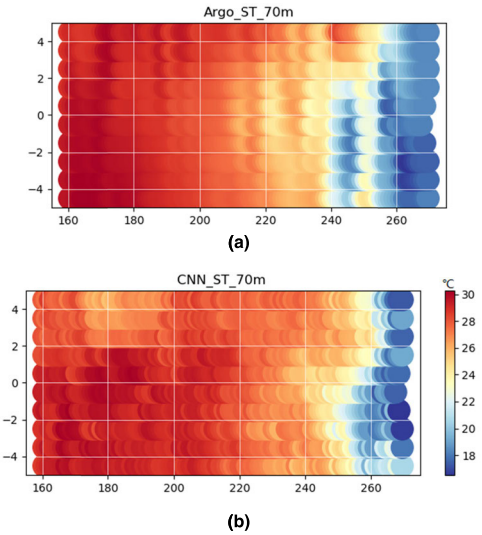

FIGURE 11. Central and eastern equatorial Pacific (5° S–5° N, 160° E–90° W) CNN predictions at 70 m in October 2015 and Argo-measured ST area distribution thermal map (a) (b). (Due to the sparse density between the data points, we extend the thermal range of each data point by 4°).

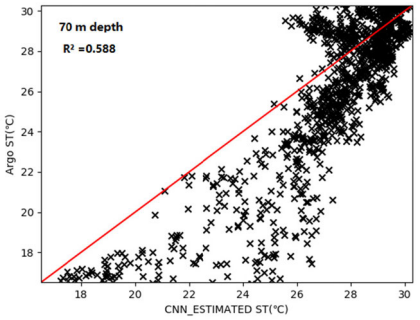

FIGURE 12. Central and eastern equatorial Pacific (5° S–5° N, 160° E–90° W) CNN predictions at 70 m in October 2015 and related Argo-measured ST area scatter plot.

by ocean currents. The MSE increases and R^2 decreases. The average MSE in July is 0.6207 (maximum/minimum is 1.8640/0.009 5 and the average R^2 is 0.942(maximum/minimum is 0.993/0.84 2 The average MSE in October is 0.8027 (maximum/minimum is 2.8232/0.0034) and the average R^2 is 0.956 (maximum/minimum is 0.983/0.939). This indicates that the forecasting ability of the CNN model is reduced in July and October is. This is mainly because the temperature of the Pacific Ocean in October fluctuates abnormally and is difficult to predict.

(2) In different years, the MSE of different depths in different months in 2004 is lower (2004 MSE average is 0.2859, 2015 MSE average is 0.5117) and R^2 is higher (2004 R^2 average is 0.969, 2015 R^2 average is 0.958) than those in 2015. The models in January, April, July and October are more reliable for the 2004 forecast but declined than those in 2015. This is mainly due to obvious climatic fluctuations and the abnormal temperature of the Pacific Ocean in recent years [27], resulting in a significant decline in the prediction accuracy of the model.

C. PARTIAL RESULT

Figure 11 and Figure 12 show the 2015 middle-eastern equatorial Pacific (5° S–5° N, 160° E–150° W, 5°S-5° N, 150°-90° W) in the area affected by El Niño events, where spatial heterogeneity is not obvious. The coefficient of determination (R^2) at 70 m is 0.588. The Argo-measured and CNN predicted thermograms behave differently in the equatorial central Pacific and eastern Pacific. The CNN model is sensitive to the new anomalies in 2015, which leads to a low prediction accuracy of the model. Table 1 and Table 2 show that in October 2015, the prediction accuracy is abnormally low, and the average mean square error (MSE) is too large. This result occurred for the following two reasons:

First, this study uses the monthly CNN model, without subtracting the climatic average of the corresponding features. Therefore, the subsurface temperature (ST) value range is

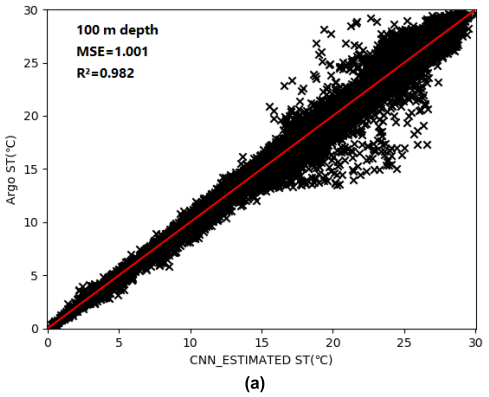

(a)

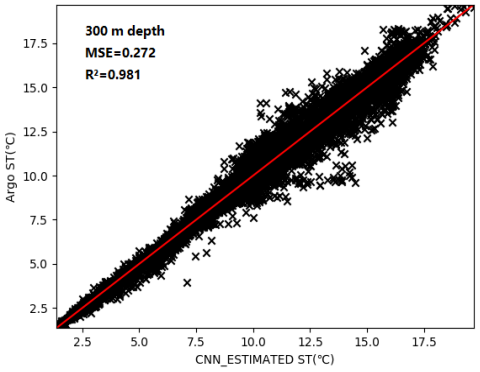

(b)

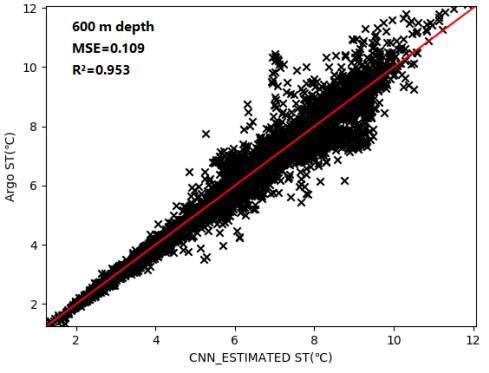

(c)

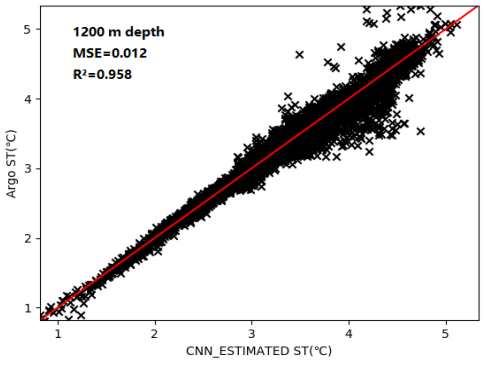

(d)

(I) 100 m(a), 300 m(b), 600 m(c), and 1200 m(d) correlation scatter plots for April 2015.

FIGURE 13. ST correlation between CNN model estimate and Argo measured values at different depths (100 m, 300 m, 600 m, and 1200 m) in different months (4(I)/10(II)).

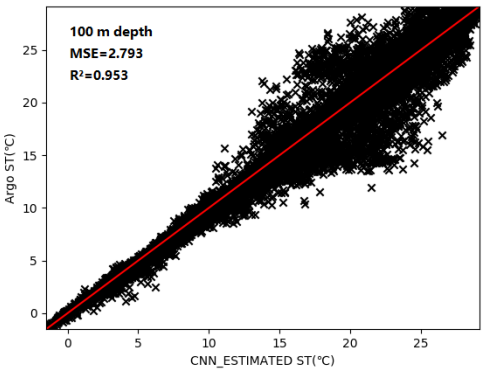

(a)

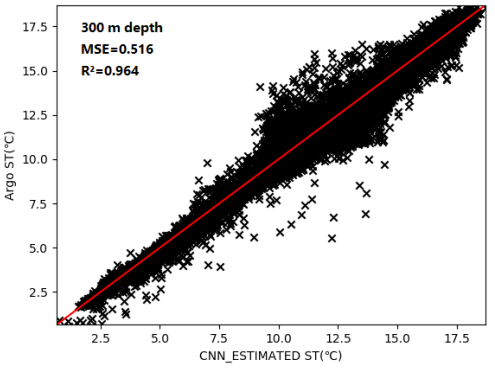

(b)

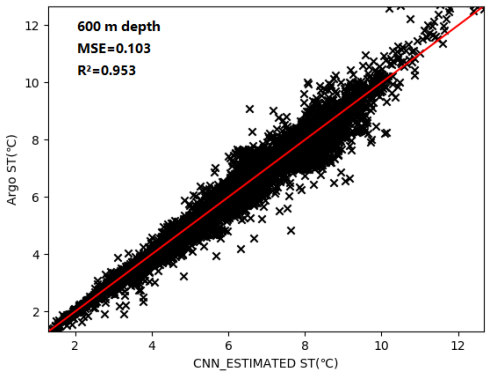

(c)

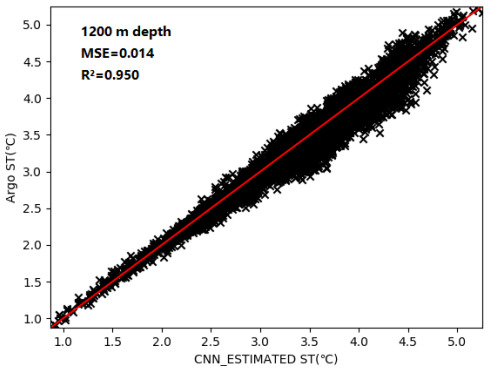

(d)

(II) 100 m(a), 300 m(b), 600 m(c), and 1200 m(d) correlation scatter plots for October 2015.

FIGURE 13. *(Continued.)* ST correlation between CNN model estimate and Argo measured values at different depths (100 m, 300 m, 600 m, and 1200 m) in different months (4(I)/10(II)).

large, resulting in a large overall MSE. However, as shown in Tables 1 and 2, the coefficient of determination (R^2) is highly accurate; that is, the model prediction accuracy is high.

Second, the strong El Niño events in 2015 caused the seawater temperature to expand westward, which led to warming of the sea surface at the equator and in the eastern Pacific Ocean. The ocean subsurface, especially the thermocline, was greatly affected by sea surface temperature. Especially for the October El Niño events, the accuracy of the CNN predictions reached the lowest point (MSE maximum value was 2.8232 at 70 m), which caused the surface temperature of the local Pacific Ocean to be abnormal. The thermocline remained abnormally deep for a long period of time [28], and the MSE was greatly affected by the fluctuation of the thermocline between 30 m and 300 m.

In general, the CNN prediction models of different months constructed using the highest-correlated data points are relatively stable (the average MSE for January, April, July, and October of 2004 and 2015 are 0.2659, 0.3129,0.5318, and 0.5160, respectively), and the estimated results for the different years of 2004 and 2015 are more reliable (average MSE is 0.4066 in 2004 and 2015, and the average R^2 is 0.964). However, as the depth increases, the accuracy of the prediction also decreases.

Figure 13 shows a correlation scatter plot between the ST estimated by using the CNN model and the ST measured by Argo in April and October 2015. If the data points in the graph are more evenly and densely distributed on the contours, then the correlation between the two is higher. This again proves that as depth increases, the coefficient of determination decreases. This also proves that the monthly CNN model can better predict the Pacific Ocean ST, and the estimation results are highly reliable (the average R^2 values for January, April, July and October of 2004 and 2015 are 0.968,0.971,0.0.949, and 0.967, respectively).

V. CONCLUSION

This paper focuses on the Pacific Ocean and makes full use of surface multisource satellite observation data (SST, SSH, and SSS). Using convolutional neural network (CNN) method, the selected training feature was the surrounding data points with the center point and the 624 data points closest to the center point (625 data points, 1875 features) and 12 monthly sets of remote sensing observation models were constructed to estimate Pacific Ocean parameters. Subsurface temperature (ST above 1975 m) is verified by the measured ST from Argo, and the accuracy is evaluated by mean square error (MSE) and the coefficient of determination (R^2). The results show that the CNN-based ST estimation model constructed in this paper is stable and reliable with high precision.

This study proposes a method for predicting the underwater temperature of the central point by using data points with the center point and the 624 data points closest to the center point. The results show that the sea surface parameters SST, SSH and SSS with the 624 data points closest to the center point have a significant effect on the subsurface temperature of the central point. This also helps to improve the estimation accuracy of ST in the Pacific region.

This study builds CNN models for different months, and uses test datasets that have no relationship with the training dataset (from 2004 and 2015). The results show that the thermal anomaly fluctuation in the model is large at 0 m-300 m, which is mainly affected by ocean currents and seasonal climate, and the internal thermal anomalies of the ocean are significantly captured. By comparing the errors in each layer (18 levels) in 2004 and 2015, it is obvious that in the context of global warming and mitigation, the thermal structure of the Pacific Ocean increases abnormally each year. In addition, under the same yearly and monthly conditions, the accuracy of ST estimation at different depths also differs.

The model has a decreasing prediction accuracy from below 500 m, which is mainly due to the global ocean ST becoming increasingly small. As the seabed thermal state tends to be stable, the spatial heterogeneity of ST is not obvious.

In summary, this paper proposes a technical method based on sea surface multisource remote sensing observation data to predict the global ocean subsurface thermal anomaly, which is conducive to the development of deep-sea remote sensing technology based on deep learning. Ultimately, this method can provide remote sensing technical support for the construction of middle and deep ocean observation datasets. Such data can be used to comprehensively understand information about the internal dynamic environment of the ocean and optimize the analysis of middle-depth to deep-sea variation during current global warming.

However, our CNN model did not reach an optimal state. We speculate that by further increasing the depth of the network, the CNN will be able to more deeply explore the characteristics of ocean remote sensing surface features and subsurface temperature. In the future, we hope to further improve the prediction accuracy by continuously tuning the parameters and network layer depth.

The convolutional neural network (CNN) is limited to local field of view convolution operations, although we have added a fully connected network to try to perceive the global view but the effect is not obvious. Since the current subsurface temperature is significantly affected by the historical temperature, CNN cannot utilize the correlation before and after the feature sequence time, so there is a deficiency in processing the time series problem. In the future, we can model by combining other time series sensitive models (such as Long-short time memory), combined with local field of view, global view, and time series.

REFERENCES

[1] M. Ishii, M. Kimoto, K. Sakamoto, and S.-I. Iwasaki, "Steric sea level changes estimated from historical ocean subsurface temperature and salinity analyses," *J. Oceanogr.*, vol. 62, no. 2, pp. 155–170, 2006, doi: 10.1007/s10872-006-0041-y.

[2] X. Wu and X.-H. Yan, "Estimation of subsurface temperature anomaly in the north Atlantic using a self-organizing map neural network," *J. Atmos. Ocean. Technol.*, vol. 29, no. 11, pp. 1675–1688, 2012, doi: 10.1175/jtech-d-12-00013.1.
[3] C. Liu, A. Köhl, Z. Liu, F. Wang, and D. Stammer, "Deep-reaching thermocline mixing in the equatorial Pacific cold tongue," *Nature Commun.*, vol. 7, no. 1, 2016, Art. no. 11576, doi: 10.1038/ncomms11576.
[4] M. A. Balmaseda, K. E. Trenberth, and E. Källén, "Distinctive climate signals in reanalysis of global ocean heat content," *Geophys. Res. Lett.*, vol. 40, no. 9, pp. 1754–1759, 2013, doi: 10.1002/grl.50382.
[5] I. Khalil, P. M. Atkinson, and P. Challenor, "Looking back and looking forwards: Historical and future trends in sea surface temperature (SST) in the Indo-Pacific region from 1982 to 2100," *Int. J. Appl. Earth Observ. Geoinf.*, vol. 45, pp. 14–26, Mar. 2016, doi: 10.1016/j.jag.2015.10.005.
[6] W. Cai, G. Wang, B. Dewitte, L. Wu, A. Santoso, K. Takahashi, Y. Yang, A. Carréric, and M. J. McPhaden, "Increased variability of eastern Pacific El Niño under greenhouse warming," *Nature*, vol. 564, no. 7735, pp. 201–206, 2018, doi: 10.1038/s41586-018-0776-9.
[7] H. Su, W. Li, and X.-H. Yan, "Retrieving temperature anomaly in the global subsurface and deeper ocean from satellite observations," *J. Geophys. Res., Oceans*, vol. 123, no. 1, pp. 399–410, 2018, doi: 10.1002/2017jc013631.
[8] M. M. Ali, D. Swain, and R. A. Weller, "Estimation of ocean subsurface thermal structure from surface parameters: A neural network approach," *Geophys. Res. Lett.*, vol. 31, no. 20, 2004, Art. no. L20308, doi: 10.1029/2004gl021192.
[9] S. Guinehut, P. Y. Le Traon, G. Larnicol, and S. Philipps, "Combining Argo and remote-sensing data to estimate the ocean three-dimensional temperature fields—A first approach based on simulated observations," *J. Marine Syst.*, vol. 46, nos. 1–4, pp. 85–98, 2004, doi: 10.1016/j.jmarsys.2003.11.022.
[10] A. Takano, H. Yamazaki, T. Nagai, and O. Honda, "A method to estimate three-dimensional thermal structure from satellite altimetry data," *J. Atmos. Ocean. Technol.*, vol. 26, no. 12, pp. 2655–2664, 2009, doi: 10.1175/2009jtecho669.1.
[11] K. Patil, M. C. Deo, and M. Ravichandran, "Prediction of sea surface temperature by combining numerical and neural techniques," *J. Atmos., Ocean. Technol.*, vol. 33, no. 8, pp. 1715–1726, 2016, doi: 10.1175/jtech-d-15-0213.1.
[12] H. Su, X. Wu, X.-H. Yan, and A. Kidwell, "Estimation of subsurface temperature anomaly in the Indian Ocean during recent global surface warming hiatus from satellite measurements: A support vector machine approach," *Remote Sens. Environ.*, vol. 160, pp. 63–71, Apr. 2015, doi: 10.1016/j.rse.2015.01.001.
[13] H. Su, L. Huang, W. Li, X. Yang, and X.-H. Yan, "Retrieving ocean subsurface temperature using a satellite-based geographically weighted regression model," *J. Geophys. Res., Oceans*, vol. 123, no. 8, pp. 5180–5193, 2018, doi: 10.1029/2018jc014246.
[14] W. Lu, H. Su, X. Yang, and X.-H. Yan, "Subsurface temperature estimation from remote sensing data using a clustering-neural network method," *Remote Sens. Environ.*, vol. 229, pp. 213–222, Aug. 2019, doi: 10.1016/j.rse.2019.04.009.
[15] H. Su, X. Yang, W. Lu, and X.-H. Yan, "Estimating subsurface thermohaline structure of the global ocean using surface remote sensing observations," *Remote Sens.*, vol. 11, no. 13, p. 1598, 2019, doi: 10.3390/rs11131598.
[16] D. Chen, A. J. Busalacchi, and L. M. Rothstein, "The roles of vertical mixing, solar radiation, and wind stress in a model simulation of the sea surface temperature seasonal cycle in the tropical Pacific Ocean," *J. Geophys. Res.*, vol. 99, no. 10, pp. 20345–20359, 1994, doi: 10.1029/94jc01621.
[17] R. Ding and J. Li, "Decadal and seasonal dependence of North Pacific sea surface temperature persistence," *J. Geophys. Res., Atmos.*, vol. 114, no. 1, 2009, Art. no. D01105, doi: 10.1029/2008jd010723.
[18] V. V. Efimov, A. V. Prusov, and M. V. Shokurov, "Seasonal instability of Pacific sea-surface-temperature anomalies," *Quart. J. Roy. Meteorol. Soc.*, vol. 123, no. 538, pp. 337–356, 1997, doi: 10.1002/qj.49712353805.
[19] W. Cai, S. Borlace, M. Lengaigne, P. van Rensch, M. Collins, G. Vecchi, A. Timmermann, A. Santoso, M. J. McPhaden, L. Wu, M. H. England, G. Wang, E. Guilyardi, and F.-F. Jin, "Increasing frequency of extreme El Niño events due to greenhouse warming," *Nature Climate Change*, vol. 4, no. 2, pp. 111–116, 2014, doi: 10.1038/nclimate2100.
[20] N. Ducet, P. Y. Le Traon, and G. Reverdin, "Global high-resolution mapping of ocean circulation from TOPEX/Poseidon and ERS-1 and −2," *J. Geophys. Res., Oceans*, vol. 105, no. 8, pp. 19477–19498, 2000, doi: 10.1029/2000jc900063.
[21] R. W. Reynolds, T. M. Smith, C. Liu, D. B. Chelton, K. S. Casey, and M. G. Schlax, "Free access daily high-resolution-blended analyses for sea surface temperature," *J. Climate*, vol. 20, no. 22, pp. 5473–5496, 2007, doi: 10.1175/2007jcli1824.1.
[22] H. Li *et al.*, "Development of a global gridded Argo data set with Barnes successive corrections," *J. Geophys. Res. Oceans*, vol. 122, no. 2, pp. 866–889, 2017, doi: 10.1002/2016jc012285.
[23] K. Fukushima, "Neocognitron: A self-organizing neural network model for a mechanism of pattern recognition unaffected by shift in position," *Biol. Cybern.*, vol. 36, no. 4, pp. 193–202, Apr. 1980, doi: 10.1007/bf00344251.
[24] Y. LeCun, B. Boser, J. S. Denker, D. Henderson, R. E. Howard, W. Hubbard, and L. D. Jackel, "Backpropagation applied to handwritten zip code recognition," *Neural Comput.*, vol. 1, no. 4, pp. 541–551, 1989, doi: 10.1162/neco.1989.1.4.541.
[25] A. Krizhevsky, I. Sutskever, and G. E. Hinton, "ImageNet classification with deep convolutional neural networks," *Commun. ACM*, vol. 60, no. 2, pp. 84–90, Jun. 2012, doi: 10.1145/3065386.
[26] L. Chen, T. Li, B. Wang, and L. Wang, "Formation mechanism for 2015/16 super El Niño," *Sci. Rep.*, vol. 7, no. 1, 2017, Art. no. 2975, doi: 10.1038/s41598-017-02926-3.
[27] P. Zhai, R. Yu, Y. Guo, Q. Li, X. Ren, Y. Wang, W. Xu, Y. Liu, and Y. Ding, "The strong El Niño of 2015/16 and its dominant impacts on global and China's climate," *J. Meteorol. Res.*, vol. 30, no. 3, pp. 283–297, 2016, doi: 10.1007/s13351-016-6101-3.
[28] S. Wu, Z.-Y. Liu, J. Cheng, and C. Li, "Response of North Pacific and North Atlantic decadal variability to weak global warming," *Adv. Climate Change Res.*, vol. 9, no. 2, pp. 95–101, 2018, doi: 10.1016/j.accre.2018.03.001.

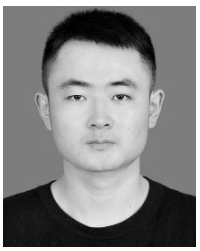

MINGXU HAN was born in China, in 1995. He received the bachelor's degree from the Chongqing University of Science and Technology, in 2018. He is currently pursuing the master's degree with the Department of Information Science and Engineering, Ocean University of China, China. His current research interests include deep learning, big data, and sensor networks.

YUAN FENG was born in China, in 1978. He received the Ph.D. degree from the Ocean University of China, Qingdao, China, in 2008. He is currently an Associate Professor with the Department of Information Science and Engineering, Ocean University of China. His main research interests are sensor networks, cloud computing, and so on.

XUELI ZHAO was born in China, in 1995. She received the bachelor's degree from Ludong University, in 2018. She is currently pursuing the master's degree with the Department of Information Science and Engineering, Ocean University of China, China. Her current research interests include deep learning and database system.

CHUNJIAN SUN received the M.A.Sc. degree from the Nanjing University of Information Science and Technology, in 2012. He is currently a Research Assistant with the National Marine Data Information Center. His research interests include ocean modeling and oceanic eddy.

FENG HONG (M'11) was born in China, in 1977. He received the Ph.D. degree from Shanghai Jiaotong University, Shanghai, China, in 2006. He is currently a Professor with the Department of Information Science and Engineering, Ocean University of China, Qingdao, China. His main research interests are sensor networks, mobile computing, and so on.

CHAO LIU was born in China, in 1988. He received the Ph.D. degree from the Ocean University of China, Qingdao, China, in 2016. He is currently an Assistant Professor with the Department of Computer Science and Technology, Ocean University of China. His main research interests include sensor networks, distributed measurement systems, and cloud computing.